Geographic ratemaking with spatial embeddings

Christopher Blier-Wong[1,3], Hélène Cossette[1,3,4], Luc Lamontagne[2,3], and Etienne Marceau[*1,3,4]

[1]*École d'actuariat, Université Laval, Québec, Canada*
[2]*Département d'informatique et de génie logiciel, Université Laval, Québec, Canada*
[3]*Centre de recherche en données massives, Université Laval, Québec, Canada*
[4]*Centre interdisciplinaire en modelisation mathématique, Université Laval, Québec, Canada*

April 28, 2021

Abstract

Spatial data is a rich source of information for actuarial applications: knowledge of a risk's location could improve an insurance company's ratemaking, reserving or risk management processes. Insurance companies with high exposures in a territory typically have a competitive advantage since they may use historical losses in a region to model spatial risk non-parametrically. Relying on geographic losses is problematic for areas where past loss data is unavailable. This paper presents a method based on data (instead of smoothing historical insurance claim losses) to construct a geographic ratemaking model. In particular, we construct spatial features within a complex representation model, then use the features as inputs to a simpler predictive model (like a generalized linear model). Our approach generates predictions with smaller bias and smaller variance than other spatial interpolation models such as bivariate splines in most situations. This method also enables us to generate rates in territories with no historical experience.

Keywords: Embeddings, territorial pricing, representation learning, neural networks, machine learning

1 Introduction

Insurance plays a vital role in protecting customers from rare but costly events. Insurance companies accept to cover a policyholder's peril in exchange for a fixed premium. For insurance costs to be fair, customers must pay premiums corresponding to their expected future costs. Actuaries accomplish this task by segmenting individuals in similar risk profiles and using historical data from these classes to estimate future costs. Advances in computation and statistical learning, along with a higher quantity of available information, drive insurance companies to create more individualized risk profiles.

An important factor that influences insurance risk is where a customer lives. Locations impact socio-demographic perils like theft (home and auto insurance), irresponsible driving (auto insurance) or quality of home maintenance (e.g., if homeowners replace the roofing regularly). Natural

---

[*]Corresponding author: Etienne Marceau, etienne.marceau@act.ulaval.ca

phenomena such as weather-based perils (flooding, hail, and storms) depend on natural factors such as elevation and historic rainfall. Geographic ratemaking attempts to capture geographic effects within the rating model. Historically, actuaries use spatial models to perform geographic ratemaking.

One may think that one must include a geographic component for a model to capture geographic effects: either depending on coordinates or on indicator variables that identify a territory. Indeed, the related research from actuarial science uses the latter approach. These models require a large quantity of data to learn granular geographic effects and do not scale well to portfolios of large territories. Until we model the geographic variables that generate the geographic risks, it is unfeasible to model postal code level risk in a country-wide geographic model. In the present paper, we propose a method to construct geographic features that capture the relevant geographic information to model geographic risk. We find that a model using these features as input to a GLM can model geographic risk more accurately and more parsimoniously than previous geographic ratemaking models.

In this paper, we construct geographic features from census data. The intuition through this paper is that since *people* generate *risk*, the geographic distribution of the *population* (as captured by census data) relates to the geographic distribution of *risk*. For this reason, we place our emphasis on constructing a model that captures the geographic distribution of the *population*, and use the results from the *population* model to predict the geographic distribution of *risk*. If we capture the geographic characteristics of the *population* correctly, then a ratemaking model using the geographic distribution of the *population* as input may not require any geographic component (coordinate or territory) since the geographic distribution of the *population* will implicitly capture some of the geographic distribution of *risk*. We focus on the geographic distribution of *populations* as an intermediate step of the predictive model. The main reason for this is that information about *populations* is often free, publicly available and smooth, while information about *risk* is expensive, private and noisy.

1.1 Spatial models

Spatial statistics is the field of science that studies spatial models. A typical problem in spatial statistics is to sample continuous variables at discrete locations in a territory and predict the value of this variable at another location within the same territory, called spatial interpolation. The prevalent theory of spatial interpolation is *regionalized variable theory*, which assumes that we can deconstruct a spatial random variable into a local structured mean, a local structured covariation, and global unstructured variance (global noise) [Matheron, 1965, Wackernagel, 2013]. To compute the pure premium of an insurance contract, it suffices to capture the local mean. Simple methods like local averaging or bivariate smoothing (local polynomial regression or splines) can compute this local mean.

A very common spatial interpolation model is called kriging [Cressie, 1990], which performs spatial interpolation with a Gaussian process parametrized by prior covariances. These covariances depend on variogram models, a tool to measure spatial autocorrelation between pairs of points as a function of distance. In our experience, variograms can be difficult to estimate in actuarial science on claims data due to the large volume of zero observed losses.

For risk management purposes, it is beneficial to study how geographic variables interact with each other. For instance, one could study the distribution of losses for an insurance contract

conditional on the fact that nearby policyholder incurred a loss. Spatial autocorrelation models study the effect of *nearness* on geographic random variables [Getis, 2010]. Spatial autoregressive models, which capture the spatial effects with latent spatial variables, are common approaches; see [Cressie, 2015] for details.

1.2 Literature review

We now review the literature of geographic ratemaking in actuarial science. One can deconstruct the spatial modeling process in three steps:

step 1 data preparation and feature engineering;
step 2 main regression model;
step 3 smoothing model or residual correction.

Early geographic models in actuarial science were correction models that smoothed the residuals of a regression model, i.e., capturing geographic effects *after* the main regression model, in a smoothing model (step 3). Notable examples include [Taylor, 1989], [Boskov and Verrall, 1994] and [Taylor, 2001]. If we address the geographic effects *during* or *before* the main regression model, then the smoothing step 3 is not required. [Dimakos and Di Rattalma, 2002] propose a Bayesian model that captures geographic trend and dependence simultaneously to the main regression model, during step 2. This model was later refined and studied as conditional autoregressive models by [Gschlößl and Czado, 2007] and [Shi and Shi, 2017]. Another approach is spatial interpolation, that capture geographically varying intercepts of the model. Examples include [Fahrmeir et al., 2003, Denuit and Lang, 2004, Wang et al., 2017, Henckaerts et al., 2018], and other spatial interpolation methods like regression-kriging [Hengl et al., 2007]. These methods use the geographic coordinates of the risk along with multivariate regression functions to capture geographic trend.

The above models capture geographic effects directly and non-parametrically, increasing model complexity and making estimation difficult (increasing the number of parameters, making them less competitive when comparing models based on criteria that penalize model complexity). As a result, geographic smoothing methods adjusted on residuals step 3 are still the prevalent geographic methods in practice for geographic ratemaking.

In the present paper, we take a fundamentally different approach, capturing the geographic effects during the feature engineering of step 1. Instead of capturing geographic effects non-parametrically with geographic models, we introduce geographic data in the ratemaking model. Geographic data is "data with implicit or explicit reference to a location relative to the Earth" [ISO 19109, 2015]. Geographic data can describe natural variables describing the ecosystem and the landform of a location, or artificial variables describing human settlement and infrastructure. We study the effectiveness of automatically extracting useful representations of geographic information with representation learning, see [Bengio et al., 2013] for a review of this field of computer science.

Early geographic representation models started with a specific application, then constructed representations useful for their applications. These include [Eisenstein et al., 2010, Cocos and Callison-Burch, 2017] for topical variation in text, [Yao et al., 2017] to predict land use, [Xu et al., 2020] for user location prediction, and [Jeawak et al., 2019, Yin et al., 2019] for geo-aware prediction. More recent approaches aim to create general geographic embeddings. These include [Saeidi et al., 2015], who use principal component analysis and autoencoders to compress census information.

In [Fu et al., 2019], [Zhang et al., 2019] and [Du et al., 2019], the authors use point-of-interest and human mobility data to construct spatial representations of spatial regions in a framework that preserves intra-region geographic structures and spatial autocorrelation. The authors use graph convolutional neural networks to train the representations. In [Jenkins et al., 2019], the authors propose a method to create representations of regions using satellite images, point-of-interest, human mobility and spatial graph data. Then, [Blier-Wong et al., 2020] propose a method that captures the geographic nature of data into a geographic data cuboid, using convolutional neural networks to construct representations using Canadian census information. The proposed model is coordinate-based, therefore more flexible than regions. [Hui et al., 2020] use graphical convolutional neural networks to compress census data in the United States to predict economic growth trends. Finally, [Wang et al., 2020] propose a framework to learn neighborhood embeddings from street view images and point-of-interest data.

2   Spatial representations

In [Blier-Wong et al., 2021a], we propose a framework for actuarial modeling with emerging sources of data. This approach separates the modeling process into two steps: a representation model and a predictive model. Using this deconstruction, we can leverage modern machine learning models' complexity to create useful representations of data and use the resulting representations within a simpler predictive model (like a generalized linear model, GLM). This section presents an overview of representation models, with a focus on spatial embeddings.

2.1   Overview of representation models

The defining characteristic of a representation model (as opposed to an end-to-end model) is that representation models never use the response variable of interest during training, relying instead on the input variables themselves or other response variables related to the insurance domain. We propose using encoder/decoder models to construct embeddings, typically with an intermediate representation (embedding) with a smaller dimension than the input data; see Figure 1 for the outline of a typical process. When training the representation model, we adjust the parameters of the encoder and the decoder, two machine learning algorithms. To construct the simpler regression model (like a GLM), one extracts embedding vectors for every observation and stores them in a design matrix.
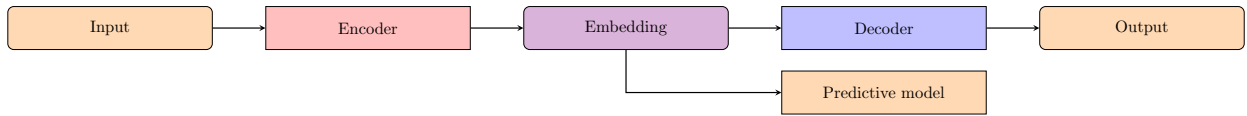

Figure 1: Encoder/decoder architecture

The representation construction process has four steps:

step 1 Construct an encoder, transforming input variables into a latent embedding vector.
step 2 Construct a decoder, which will determine which information the representation model must capture.

step 3 (Optional) Combine features from different sources into one combined embedding.

step 4 (Optional) Evaluate different embeddings, validate the quality of representations.

We now enumerate a few general advantages of the representation approach. First, representation models can transform categorical variables into dense and compact vectors, which is particularly important for territories since the cardinality of this category of variables is typically very large. Second, representation models can reduce the input variable dimension into one of our choosing: we typically select an embedding dimension much smaller than the original. Third, we can build representations such that they are useful for general tasks, so we can reuse representations. Fourth, representations can learn non-linear transformations and interactions automatically, eliminating the need to construct features by hand. Finally, when using a representation model, one can reduce the regression model's complexity. If the representation model learns all useful interactions and non-linear transformations, a simple model like a GLM could replace more complex models like end-to-end gradient boosting machines or neural networks.

2.2 Motivation for geographic embeddings

The geographic methods proposed in actuarial science (see the literature review) address the data's geographic nature at step 2 and step 3 of geographic modeling. Geographic embeddings are a fundamentally different approach to geographic models studied in actuarial science. We first transform geographic data into geographic embedding vectors, during feature engineering (step 1). By using geographic embeddings in the main regression model, we capture the geographic effects and the traditional variables at the same time. Figure 2 provides an overview of the method. The representation model takes geographic data as input to automatically create geographic features (geographic embeddings). Sections 3 and 4 respectively present architectures and implementations of geographic embedding models. Then, we combine the geographic embeddings with other sources of data (for example, traditional actuarial variables like customer age). Finally, we use the combined feature vector within a predictive model.
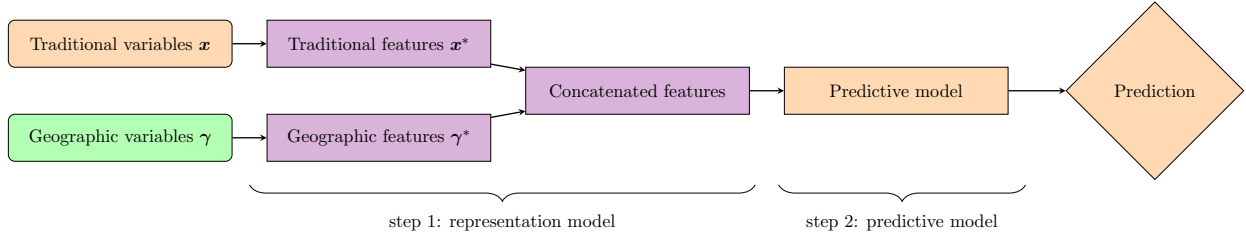

Figure 2: Proposed geographic ratemaking process

The representation model's complexity does not affect the predictive model's since the representation model is *unsupervised* with respect to the predictive task. We can construct representation models that are highly non-linear with architectures that capture the unique characteristics of different data sources. This model will induce geographic effects into embeddings while capturing the desirable characteristics of geographic models. In most cases, regression models (GLMs) using these geographic embeddings as inputs will have lower variance and often lower bias than geographic models, as demonstrated with examples in Section 5.

In [Blier-Wong et al., 2021a], the authors present a collection of tools to construct useful ac-

tuarial representations. Section 7 of that paper deals with geographic representation ideas. The present paper aims to pursue our investigation on geographic representations for actuarial science by providing an implementation and an application.

The representation learning framework enables one to select an architecture that captures specific desirable attributes from various data sources. There is one generally accepted desirable attribute for geographic models, called Tobler's first law (TFL) of geography. We also propose two new attributes that make geographic embeddings more useful, based on our experience with geographic models. Below is a list of these three desirable attributes for geographic embeddings.

Attribute 1 (TFL) *Geographic embeddings must follow Tobler's first law of geography.* As mentioned in [Tobler, 1970], "everything is related to everything else, but near things are more related than distant things". This attribute is at the core of spatial autocorrelation statistics. Spatial autocorrelation is often treated as a confounding variable, but these variables constitute information since it captures how territories are related (see, e.g., [Miller, 2004] for a discussion). A representation model, capturing the latent structure of underlying data, generates geographic embeddings.

Attribute 2 (coordinate) *Geographic embeddings are coordinate-based.* A coordinate-based model depends only on the risk's actual coordinates and its relation to other coordinates nearby. Polygon-based models highly depend on the definition of polygon boundaries, which could be designed for tasks unrelated to insurance.

We motivate this attribute with an example. Consider four customers A, B, C and D, that have home insurance for their house in the island of Montréal, Québec, Canada. Figure 3 identifies each coordinate on a map. We also included the borders of polygons, represented by bold black lines. These polygons correspond to Forward Sortation Areas (FSA), a unit of geographic coordinate in Canada (further explained in Section 4). Observations A and B belong to the same polygon, while observations B and C belong to different ones. However, B is closer to C than to A. Polygon-based representation models and polygon-based ratemaking models assume that the same geographic effect applies to locations A and B, while different geographic effects apply to locations B and C. However, following TFL, one expects the geographic risk between customers B and C to be more similar than the geographic risk between A and B.

There are two other issues with the use of polygons. The first is that the actual shapes of polygons could be designed for purposes that are not relevant for capturing geographic risk (for example, postal codes are typically optimized for mail distribution). If an insurance company uses polygons for geographic ratemaking, it is crucial to verify that risks within each polygons are geographically homogeneous. The second issue is that polygon boundaries may change in time. If postal codes are split, moved, merged or created, the geographic ratemaking model will also split, move, merge the territories, and be unable to predict for newly created postal codes. A customer living at the same address could see its insurance premium drastically increase or decrease due to the arbitrary change in polygon boundary, even if there is no actual change in the geographic risk.

Finally, the type of location information (coordinate or polygon) for the ultimate regression task may be unknown while training the embeddings. For this reason, one should not make the polygon depend on a specific set of boundary polygon shapes. On the other hand, one can easily aggregate coordinates into the desired location type for the ultimate regression task.

Attribute 3 (external) *Geographic embeddings encode relevant external information.* There are two reasons for using external information. The first is that geographic effects are complex, so we
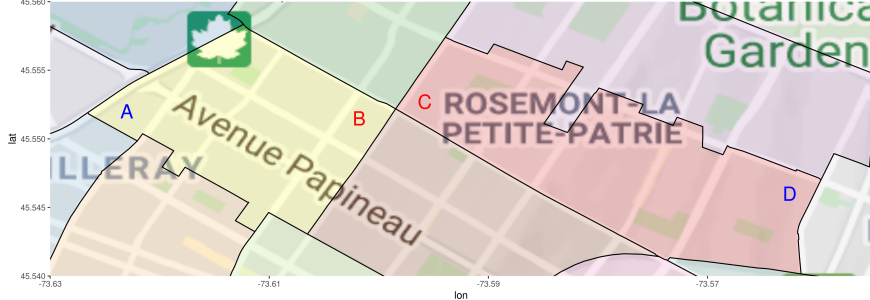
Figure 3: Coordinates vs polygons

need a large volume of geographic information to capture the confounding variable that generates them. Constructing geographic embeddings with a dataset external to one's specific problem may increase the quantity and quality of data, providing new information for spatial prediction. The second reason is that geographic embeddings can produce rates in territories with no historical loss experience, as long as we have external information for the new territory. Traditional geographic models capture geographic effects from experience but are useless to rate new territories. If we train geographic embeddings on external datasets that cover a wider area than the loss experience of an insurance company, we may use the geographic embeddings to capture geographic effects in territories with no loss experience. This second reason is related to using one-hot encodings of territories; see [Blier-Wong et al., 2021a] for further illustrations. Finally, the external information should be relevant to the insurance domain. Although geographic embeddings could be domain agnostic (general geographic embeddings for arbitrary tasks), our ultimate goal is geographic ratemaking, so we select the external information that is related to causes of geographic risks.

To construct the geographic representations, we use a flexible family of machine learning methods called deep neural networks. In the past few years, actuarial applications of neural networks are increasing in popularity; see [Richman, 2020, Blier-Wong et al., 2021b] for recent reviews. We construct the neural networks such that the representations satisfy the three desirable attributes of geographic embeddings, so any predictive model (even linear ones) using the geographic embeddings as input will also satisfy the desirable attributes.

2.3 Relationship with word embeddings

The geographic embeddings approach that we propose is largely inspired by word embeddings in natural language processing (NLP). The fundamental idea of word embeddings dates back to linguists in the 1950's. On the subject of the distributional hypothesis and synonyms, [Harris, 1954] states "If A and B have some environments in common and some not ... we say that they have different meanings, the amount of meaning difference corresponding roughly to the amount of difference in their environments." Although this *environment* refers to the context of a word within text, this same quote applies to geography. Another justification that resembles TFL comes from [Firth, 1957], stating "You shall know a word by the company it keeps!"

Words and territories are also similar since one represents them as categorical variables with a large cardinality. For this reason, it isn't surprising that the classical models for NLP tasks and geographic prediction are similar. Simple representations of text like bag-of-words and n-grams

are similar to simple representations of territories like one-hot encodings. Further techniques use smoothing to account for unknown words or territories, while more sophisticated methods use graphical models like hidden Markov models or conditional autoregressive models to account for textual or geographic autocorrelation. Most recent models in NLP use word embeddings [Mikolov et al., 2017], and researchers are starting to study geographic embeddings. Table 1 summarizes the comparisons outlined in this paragraph.

	NLP	Geography
Fondamental justification	Distributional hypothesis [Harris, 1954, Firth, 1957]	Tobler's first law of geography [Tobler, 1970]
Classical tools & techniques	Bag-of-words & n-grams n-gram smoothing (Laplace) Hidden Markov models	One-hot encoding of territories Smoothing (kriging, splines) Conditional autoregressive models
Representation techniques	Word embeddings [Mikolov et al., 2013] [Devlin et al., 2019]	Geographic embeddings [Fu et al., 2019], [Blier-Wong et al., 2020]

Table 1: Comparing contributions and techniques for NLP and geographic models

Attribute 2 proposes to use coordinates instead of polygons to construct geographic embeddings. This is analogous to using character-level embeddings instead of word embeddings. NLP researchers use character-level embeddings to understand the semantics of an unknown word (a word which we never saw in a training corpus).

The principal difference between words and territories is that territories are not interchangeable or synonymous. Instead, we capture the co-occurrence of relevant geographic information, see attribute 3.

3   Convolution-based geographic embedding model

In this section, we describe an approach to construct geographic embeddings. We will explain the representation model choices for the encoder in step 1, the decoder in step 2 and the evaluation in step 4. For the embeddings to have all desirable attributes of geographic embeddings enumerated in the previous section, we must modify the process to account for geographic data, adding a data preparation step. Our focus is on constructing a geographic representation model, so we omit the (optional) step 3 of combining representations with other sources of data in this section.

3.1   Preparing the data

Suppose we are interested in creating a geographic feature that characterizes a location **s**. Following attribute 3 (external), we must first collect geographic information for location **s**. Objects characterized by their location in space can be stored as point coordinates or polygons (boundary coordinates) [Anselin et al., 2010]. Point coordinate data corresponds to the measurements of a variable at an individual location. It can indicate the presence of a phenomenon (set of locations where accidents occurred) or the measurement of a variable at a particular location (age of a building at a location) [Diggle, 2013]. Polygon data aggregates variables from all point patterns in a

territory. In Figure 3, the individual marks A, B, C and D are point patterns, and the different shaded areas are polygons.

To construct the representation model, we assume that we have one or many external datasets in polygon format, with a vector of data for each polygon. This is the case for census data in North America. Suppose the coordinate of $\mathbf{s}$ is located within the boundaries of polygon $\mathbf{S}$, then one associates the external geographic data from polygon $\mathbf{S}$ to location $\mathbf{s}$. We will use the notation $\boldsymbol{\gamma} \in \mathbb{R}^d$ to denote the vector of geographic variables.

In usual (non-spatial) situations, the type and format of data determines the topology of the encoder. Geographic information is often vectorial (called spatial explanatory variables [Diggle and Ribeiro, 2007]) so that the associated neural network encoder would be a fully-connected neural network. A fully-connected neural network encoder would satisfy the *external* attribute, but not *TFL* or *coordinate*. To understand why the *coordinate* is not entirely satisfied, we consider one external data source from one set of polygons. In this case, observations within the same polygon will have the same geographic variables $\boldsymbol{\gamma}$, so the geographic data remains polygon-based. Instead, we modify the input data for the representation model to satisfy the *TFL* and *coordinate* attributes. To create an embedding of location $\mathbf{s}$, we will not only use information from location $\mathbf{s}$, but also data from surrounding locations. Since each coordinate within a polygon may have different surrounding locations, the resulting embeddings will not be polygon-based, satisfying the *coordinate* attribute.

An approach to satisfy *TFL* is to use an encoder that includes a notion of nearness. Convolutional neural networks (CNNs) have the property of sparse interactions, meaning the outputs of a convolutional operation are features that depend on local subsets of the input [Goodfellow et al., 2016]. CNNs accept matrix data as input. For this reason, we will define our neighbors to form a grid around a central location. The representation model's input data is the geographic data square cuboid from [Blier-Wong et al., 2020], which we present in Algorithm 1 and explain below. One notices that the geographic data square cuboid is a specific case of a multiband raster, datacube or multidimensional array.

To create the geographic data cuboid for a location $\mathbf{s}$ with coordinate (lon, lat), we span a grid of $p \times p$ neighbors, centered around (lon, lat). Each neighbor in the grid is separated horizontally and vertically by a distance of w. The steps 1 to 4 of Algorithm 1 create the matrix of coordinates for the neighbors, and we illustrate each transformation in Figure 4.

(a) Unit grid   (b) Scale   (c) Rotate   (d) Translate
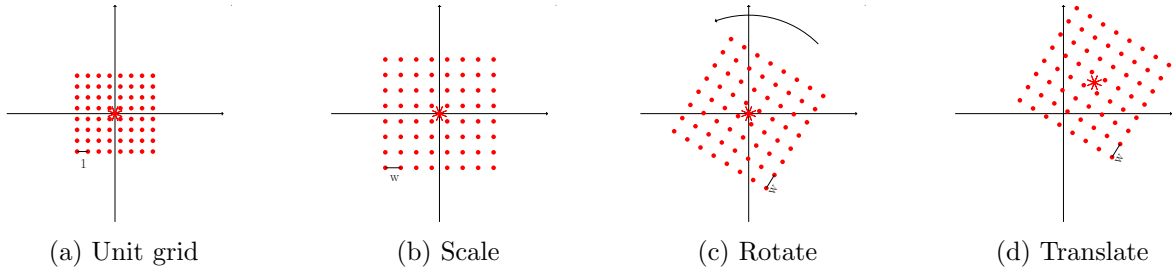
Figure 4: Creating the grid of neighbors

Each coordinate in δ has geographic variables $\boldsymbol{\gamma} \in \mathbb{R}^d$, extracted from different external data sources of polygon data. The set of variables for every location in δ, which we note $\underline{\boldsymbol{\gamma}}_\delta$, forms a square cuboid of dimension $p \times p \times d$, which we illustrate in Figure 6. We can interpret the geographic data square cuboid as an image with d channels, with one channel for each variable. Algorithm 1 presents the steps to create the data square cuboid for a single location. Lines 1 to

---
Algorithm 1: Generating a geographic data square cuboid

Input: Center coordinate (lon, lat), width w, size p, geographic data sources
Output: Geographic data square cuboid

1 generate empty grid of dimension $p \times p$ and width 1 with the set

$$\bigcup_{k=0}^{p-1} \bigcup_{j=0}^{p-1} \left[\frac{1}{2}(2k - p + 1), \ \frac{1}{2}(2j - p + 1) \right],$$

store the coordinates of this set of points in a matrix δ_0 (each column is a coordinate, the first row is the longitude, the second row is the latitude);

2 scale (multiply) by w;

3 sample $\theta \sim Unif(0, 360)$ and rotate the scaled matrix, $R(w\delta_0) = w \begin{pmatrix} \cos\theta & -\sin\theta \\ \sin\theta & \cos\theta \end{pmatrix} \delta_0$;

4 translate matrix by $(lon, lat)'$, to get $\delta = R(w\delta_0) + \begin{pmatrix} lon \\ lat \end{pmatrix}$;

5 **foreach** *external geographic data source* **do**
6   **foreach** *coordinate in δ* **do**
7   allocate coordinate to corresponding polygon index;
8   append vector data to current coordinate
---

4 generate the set δ for the center location (the matrix of neighbor coordinates), while lines 4 to 7 fill each coordinate's variables. The random rotation is present such that our model does not exclusively learn effects in the same orientation.
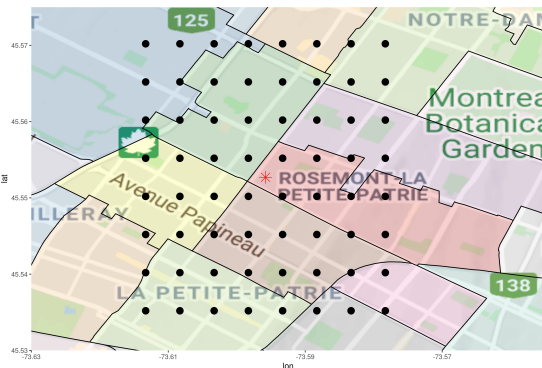
Figure 5: Set of neighbor coordinates δ
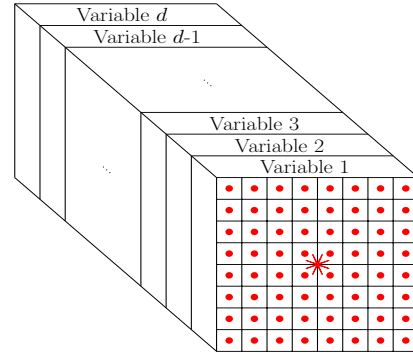
Figure 6: Data square cuboid $\underline{\gamma}_\delta$

If the grid size p is even, δ does not include the center coordinate (lon, lat). This means the geographic data square cuboid depends only on neighbor information and not information of the center point itself.

3.2 Constructing the encoder

As explained in Section 2.1, the encoder generates a latent representation from a bottleneck, which we then extract as embeddings. Above, we constructed the input data to have a square cuboid shape to use convolutional neural networks as an encoder. The encoder has convolutional operations, reducing the size of the hidden square cuboids (also called feature maps in computer vision) after each set of convolutions. Then, we *unroll* (from left to right, top to bottom, front to back, see Figure 7 for an illustration) the square cuboid into a vector. The unrolled vector will be highly autocorrelated: since the output of the convolutions includes local features, features from the same convolutional layer will be similar to each other, causing collinearity if we use the unrolled vector directly within a GLM. For this reason, we place fully-connected layers after the unrolled vector. The last fully-connected layer of the encoder is the geographic embedding vector, noted γ^*. This layer typically has the smallest dimension of the entire neural network representation model. For a geographic embedding of dimension ℓ, then the encoder will be a function $\mathbb{R}^{p \times p \times d} \to \mathbb{R}^{\ell}$.
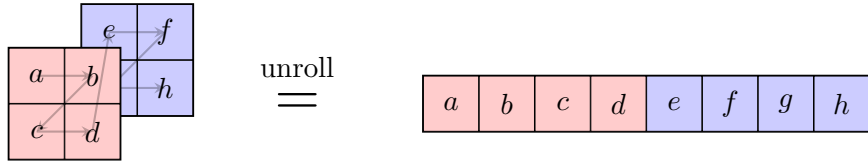

Figure 7: Unrolling example for a $2 \times 2 \times 2$ cuboid. Different colors are different variables

We have now constructed the encoder for our representation model. This encoder satisfies desirable attributes 1 to 3 since

1. the encoder is a convolutional neural network, which captures sparse interactions from neighboring information, encoding the notion of nearness;
2. the embeddings are coordinate-based: as the center coordinate moves, the neighboring coordinates also move, so center coordinates within the same polygon may have different geographic data square cuboids;
3. the model uses external data as opposed to one-hot encodings of territories.

3.3 Constructing the decoder

The decoder guides the type of information that the embeddings encode, i.e., selects which domain knowledge to induce into the representations, see Section 2.1 for details on the decoding procedure. If one has response variables related to the insurance domain for the whole dataset (i.e., for all coordinates within the territory for which we construct embeddings), we could train the decoder with transfer learning, such that the representation model learns important information related to insurance. In our case, the external dataset that covers Canada, and we do not have insurance statistics over the entire country. For this reason, our decoder will attempt to predict itself, i.e., the input variables γ.

The original model for geographic embeddings we explored was the convolutional regional autoencoder (CRAE), presented in [Blier-Wong et al., 2020]. The input of CRAE is the geographic data cuboid, and the output is also the geographic data cuboid. The neural network architecture is called a convolutional autoencoder since the model's objective is to reconstruct the input data after going through a bottleneck of layers. The decoder in CRAE is a function $\mathbb{R}^{\ell} \to \mathbb{R}^{p \times p \times d}$. One

can interpret CRAE as *using contextual variables to predict the same contextual variables*. The loss function for CRAE is the average reconstruction error. For a dataset of N coordinates, the loss function is

$$\mathcal{L} = \frac{1}{N} \sum_{i=1}^{N} \left|\left| g\left(f\left(\underline{\boldsymbol{\gamma}}_{\delta_i}\right)\right) - \underline{\boldsymbol{\gamma}}_{\delta_i} \right|\right|^2, \tag{1}$$

where f is the encoder, g is the decoder, $\underline{\boldsymbol{\gamma}}_{\delta_i} \in \mathbb{R}^{p \times p \times d}$ is the geographic data cuboid for the coordinate of location i and $||\cdot||$ is the euclidean norm. However, attribute 2 only requires information from the grid's central location, not the entire grid. Therefore, much of the information contained within CRAE embeddings captures irrelevant or redundant information.

In this paper, we improve CRAE by changing the decoder. One can interpret the new model as using *contextual variables to predict the central variables*, directly satisfying the *coordinate* attribute. This same motivation was suggested for natural language processing in [Collobert and Weston, 2008] and applied in a model called Continuous Bag of Words (CBOW) [Mikolov et al., 2013]. Instead of reconstructing the entire geographic data cube, the decoder attempts to predict the variables $\boldsymbol{\gamma}$ for location $\mathbf{s}$. Therefore, the decoder is a series of fully-connected layers that act as a function $\mathbb{R}^{\ell} \to \mathbb{R}^{d}$, where $\ell \ll d$. The loss function for CBOW-CRAE is also the average reconstruction error, but on the vector of variables for the central location instead on the entire geographic data square cuboid:

$$\mathcal{L} = \frac{1}{N} \sum_{i=1}^{N} \left|\left| g\left(f\left(\underline{\boldsymbol{\gamma}}_{\delta_i}\right)\right) - \boldsymbol{\gamma}_i \right|\right|^2. \tag{2}$$

Figure 8 illustrates the entire convolution-based model architecture of CBOW-CRAE.
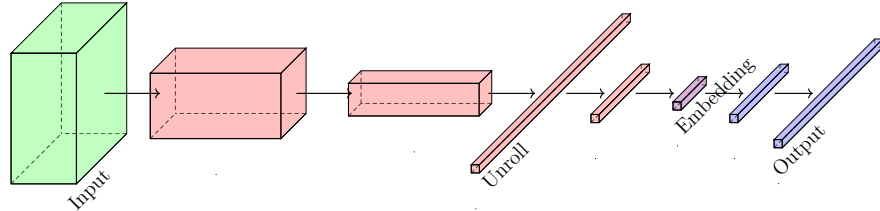
Figure 8: Convolution-based geographic embedding model

3.4 Evaluating representations

There are two types of evaluations for embeddings: the most important are extrinsic evaluations, but intrinsic evaluations are also significant [Jurafsky and Martin, 2009]. One evaluates embeddings extrinsically by using them in downstream tasks and comparing their predictive performance. In P&C actuarial ratemaking, one can use the embeddings within ratemaking models for different lines of business and select the embedding model that minimizes the loss on out-of-sample data.

According to our knowledge, there are no intrinsic evaluation methods for geographic embeddings. We propose one method in this paper and discuss other approaches in the conclusion. Intrinsic evaluations determine if the embeddings behave as expected. To evaluate embeddings intrinsically, one can determine if they possess the three attributes proposed in Section 2. Due to

the geographic data cuboid construction, geographic embeddings already satisfy attributes *coordinate* and *external*, so these attributes do not need intrinsic evaluations. To validate *TFL*, we can plot individual dimensions of the embedding vector on a map. Embeddings that satisfy *TFL* vary smoothly, and one can inspect this property visually. Section 4.7 presents the implicit evaluation for the implementation on Canadian census data.

4   Implementations of geographic embeddings

In this section, we present an implementation of geographic embeddings using census data in Canada. We select census data since they contain crucial socio-demographic information on the customer's geography; geographic embeddings trained with census data will compress this information. One could also use natural (ecosystem, landform, weather) information to create geographic embeddings that capture natural geographic risk. We first present the census data in Canada, along with issues related to some of its characteristics. Then, we explain the architectural choices and implementations for the geographic data square cuboid, the encoder and the decoder. Finally, we perform intrinsic evaluations of the geographic embeddings.

Our strategy for constructing geographic embeddings contains two types of hyperparameters: general neural network hyperparameters, and specific hyperparameters related to the particular model architecture. *General hyperparameters* control the method used to optimize the neural network parameters, especially the optimization routine: these include the choice of the optimizer, the batch size, the learning rate, the weight decay, the number of epochs and the patience for the learning rate reduction. We select general hyperparameters using grid-search, along with personal experience with neural networks. We refer the reader to other texts such as [Goodfellow et al., 2016] for general tips on hyperparameter search. We will limit our discussion of general hyperparameter search to mentioning the optimal parameters that we use. *Specific hyperparameters* are associated with the specific neural network architecture and includes the square cuboid width w and the pixel size p to generate a geographic data square cuboid. Other specific hyperparameters determine the neural network architecture, including the shape and depth of convolutions and fully connected layers. Tuning these hyperparameters requires experience with neural networks since the combinations of specific hyperparameters are much too large to determine using grid-search. We will explain our thought process: starting with accepted heuristics, then manually exploring the hyperparameter space to determine the optimal architecture.

4.1   Canadian census data

We now present some characteristics of Canadian census data. Statistics Canada publishes this data every five years, and our implementation uses the most recent version (2016). The data is aggregated into polygons called forward sortation areas, which correspond to the first three characters of a Canadian postal code; see Figure 9 for the decomposition of a postal code. Statistics Canada aggregates the public release of census data to avoid revealing confidential and individual information. The data is also available at the dissemination area polygon level, which is more granular than FSA. We work with FSAs because they are simpler to explain. There are 1 640 FSAs in Canada, and each polygon in Figure 5 represents a different FSA. The grid of neighbor coordinates of Figure 5 contains 8 points from the same FSA as the central location, represented by the red star.

$$\overset{\text{Postal district}}{\underbrace{\overbrace{\text{H2T}}^{} \underbrace{\text{1W8}}_{\text{LDU}}}_{}}$$

$$\underbrace{\text{H2T}}_{\text{FSA}} \underbrace{\text{1W8}}_{\text{LDU}}$$
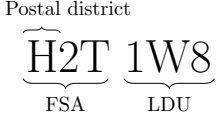
Figure 9: Deconstruction of a Canadian postal code

The first issue with using census data for insurance pricing is the use of protected attributes, i.e., variables that should legally or ethically not influence the model prediction. One example is race and ethnicity [Frees, 2015]. Territories may exhibit a high correlation with protected attributes like ethnic origin. To construct the geographic embeddings, we discard all variables related to ethnic origin (country of origin, mother tongue, citizen status). We retrain only variables that a Canadian insurance company could use for ratemaking. In Appendix A, we provide a complete list of the categories of variables within the census dataset, and we denote with an asterisk the categories of variables that we omit. What remains is information about age, education, commute, income and others, and comprises 512 variables that we denote γ. Removing protected attributes from a model is a technique called anti-classification [Corbett-Davies and Goel, 2018], or fairness through unawareness [Kusner et al., 2018], which does not eliminate discrimination entirely and in some cases may increase it [Kusner et al., 2018]. Studying discrimination-free methods to construct geographic embeddings is kept as future work. For analysis and discussion of discrimination in actuarial ratemaking, see [Lindholm et al., 2020].

It is common practice in machine learning to normalize input variables such that they are all on the same scale. Two reasons are that stochastic gradient-based algorithms typically converge faster with normalized variables, and un-normalized variables have different impacts on the regularization terms of the loss function [Shalev-Shwartz and Ben-David, 2014]. For autoencoders, an additional reason is that the model's output is the reconstruction of many variables, so variables with a higher magnitude will generate a disproportionately large reconstruction error relative to other variables (so the model will place more importance on reconstructing these variables). Normalization requires special attention for aggregated variables like averages, medians, and sums: some must be aggregated with respect to a small number of observations, others with respect to the population within the FSA of interest and others with the Canadian average. For example, the FSA population is min-max normalized (see [Han et al., 2011]) with respect to all FSAs in Canada. For age group proportions (for instance, the proportion of 15 to 19-year-olds), we normalize with respect to the current FSA's population size.

When using Algorithm 1, some coordinates do not belong to a polygon index, which happens when the coordinate is located in a body of water. To deal with this situation, we created a vector of missing values filled with the value 0.

Finally, we project all coordinates to Atlas Lambert [Lambert, 1772, Snyder, 1987] to reduce errors when computing distances. Due to Earth's curvature, computing Euclidean distance with degree-based coordinates like GPS underestimates distances; see [Torge and Müller, 2012] for illustrations. When changing the coordinate system to Atlas Lambert, one can compute distances using traditional euclidean metrics with greater accuracy.

4.2   Geographic data square cuboid

Now that we have prepared the census data, we can construct the geographic data cuboid for our implementation. The parameters for the geographic data square cuboid include square width w and pixel size p. One can interpret these values as smoothing parameters. The square width w affects the geographic scale of the neighbors, while the pixel size p determines the density of the neighbors. For very flexible embeddings, one can choose small w so that the geographic embeddings will capture local geographic effects. If the embeddings are too noisy, then one can increase p to stabilize the embedding values. Ultimately, the importance is the span of the grid, determined by the farthest sampled neighbors. For an even value of w, the closest sampled neighbor coordinates are the four corners surrounding the central location at a distance of $p/\sqrt{2}$ units from the central location. The farthest sampled neighbors are the four outermost corners of the grid at a distance of $p(w-1)/\sqrt{2}$ units. Selecting the best parameters is a tradeoff between capturing local variations in densely populated areas and smoothing random fluctuations in rural areas. Insurance companies could construct embeddings for rural portfolios and urban portfolios with different spans to overcome this compromise. Another solution consists of letting the parameters depend on local characteristics of the population, such as population density (select parameters such that the population contained within a grid is above a threshold) or the range of a variogram (select parameters such that the observations within the grid still exhibit geographic autocorrelation).

We consider square widths of $w = \{8, 16\}$ and pixel sizes of $p = \{50, 100, 500\}$ meters. Our experiments showed that a square width of $w = 16$ and a pixel size of $p = 100$ meters produced smaller reconstruction errors. The geographic data square cuboid then samples $16^2 = 256$ neighbors, the closest one being at a distance of 71 meters and the farthest one at 1061 meters from the center location. Since we have 512 features available for every neighbor, the size of the input data is $16 \times 16 \times 512$ and contains 131 072 values.

The dataset used to train the representation models is composed of a geographic data square cuboid for every postal code in Canada (888 533 by the time of our experiments). A dataset containing the values of every geographic data square cuboid would take 2To of memory, too large to hold in most personal computers. For this reason, we could not generate the complete dataset. However, one can still train geographic embeddings on a personal computer by leveraging the fact that many values in the dataset repeat. For each postal code, one generates the grid of neighbor coordinates (steps 1 to 4 of Algorithm 1) and identifies the corresponding FSA for each coordinate (step 6 of Algorithm 1). We then unroll the grid from left to right and from top to bottom into a vector of size 256. For memory reasons, we create a numeric index for every FSA (A0A = 1, A0B = 2, ..., Y1A = 1 640), and store the list of index for every postal code in a CSV file (1GB). Another dataset contains the normalized geographic variables $\boldsymbol{\gamma}$ for every FSA (15.1MB). Most modern computers can load both datasets in RAM. During training, our implementation retrieves the vector from the index and retrieves the values associated with each FSA (step 8 of Algorithm 1), then rolls the data into geographic data square cuboids.

4.3   Encoders

This subsection will detail specific architecture choices for encoders with Canadian census data, presenting two strategies to determine the optimal architecture. Each contains two convolution layers with batch normalization [Ioffe and Szegedy, 2015] and two fully-connected layers. Strategy 1 reduces the feature size between the last convolution layer and the first fully-connected layer, while

strategy 2 reduces the feature size between convolution layers. Each encoder uses a hyperbolic tangent (tanh) activation function after the last fully-connected layer to constrain the embedding values between -1 and 1. After testing convolutional kernels of size $k = \{3, 5, 7\}$, the value $k = 3$ resulted in the lowest reconstruction errors.

4.3.1 Strategy 1

A popular strategy for CNN architectures is to reduce the width and height but increase the depth of intermediate features as we go deeper into the network, see [Simonyan and Zisserman, 2014, He et al., 2016]. The first strategy follows three heuristics:

1. Apply half padding, such that the output dimension of intermediate convolution features remains the same.
2. Apply max-pooling after each convolution step with a stride and kernel size of 2, reducing the feature size by a factor of 4.
3. Double the square cuboid depth after each convolution step.

The result of this strategy is that the size (the number of features in the intermediate representations) is reduced by two after every convolution operation. We present the square cuboid depth and dimension at all stages of the models in Table 2. The feature size (row 3) is the product of square cuboid depth (number of channels) and the dimension of the intermediate features. In strategy 1,

	Input	Conv1	Conv2	Unroll	FC1	FC2
Square cuboid depth	512	1 024	2 048	32 768	128	16
Square cuboid width $\times$ height	16×16	8×8	4×4	1	1	1
Feature size	131 072	65 536	32 768	32 768	128	16
% of parameters	NA	17	68	NA	15	0

Table 2: Large encoder model with 27 798 672 parameters

the convolution step accounts for most parameters. The steepest decrease in feature size occurs between the second convolution block and the first fully-connected layer (from 32 768 to 128).

4.3.2 Strategy 2

For the second strategy, we follow a trial and error approach and attempt to restrict the number of parameters in the model. We retain heuristics 1 and 2 from strategy 1, but the depth of features decrease between each convolution block.

	Input	Conv1	Conv2	Unroll	FC1	FC2
Square cuboid depth	512	48	16	256	16	8
Square cuboid width $\times$ height	16×16	8×8	4×4	1	1	1
Feature size	131 072	3 072	256	256	16	8
% of parameters	NA	95	3	NA	2	0

Table 3: Small encoder model with 232 514 parameters

In strategy 2, 95% of the parameters are in the first convolution step. The feature size decreases steadily between each operation.

4.4 CRAE & CBOW-CRAE decoders

The output for the CRAE model is the reconstructed geographic data cuboid. The decoder in this model is the inverse operations of the encoder (deconvolutions and max-unpooling). The final activation function is sigmoid because the original inputs are between 0 and 1. We present the decoder operations for the large and the small decoders in Tables 4 and 5. Recall that the input to the decoder is the embedding layer from the encoder.

	Input	FC3	FC4	Roll	Deconv1	Deconv2
Square cuboid depth	16	128	32 768	2 048	1 024	512
Square cuboid width × height	1	1	1	4×4	8×8	16×16
Feature size	16	128	32 768	32 768	65 536	131 072
% of parameters	NA	0	15	NA	68	17

Table 4: Large CRAE decoder model

	Input	FC3	FC4	Roll	Deconv1	Deconv2
Square cuboid depth	8	16	256	16	48	512
Square cuboid width × height	1	1	1	4×4	8×8	16×16
Feature size	8	16	256	256	3 072	131 072
% of parameters	NA	91	3	NA	2	0

Table 5: Small CRAE decoder model

The CBOW-CRAE is a context to location model, so we select a fully-connected decoder, increasing from the embedding (γ^*) size ℓ to the geographic variable (γ) size d. In our experience, the decoder's exact dimensions did not significantly impact the reconstruction error, so we select the ascent dimensions (FC3 and FC4) to be the same as the fully-connected descent dimensions (FC1 and FC2). When there is no hidden layer from the embedding to the output (if there is only one fully-connected layer), the model is too linear to reconstruct the input data. When there is one hidden layer, the model is mainly able to reconstruct the data. Additional hidden layers did not significantly reduce the reconstruction error, so we select only one hidden layer in the decoder. Table 6 presents the CBOW CRAE decoders in our implementation.

	Input	FC3	FC4
Small model	8	16	512
Large model	16	128	512

Table 6: CBOW-CRAE decoders

4.5 Comments on general hyperparameters and optimization strategy

We now offer a few comments on the training strategy. We split the postal codes into a training set and a validation set. Since the dataset is very large, we select a test set composed of only 5% of the postal codes. We train the neural networks on a GeForce RTX 2080 8 GB GDDR6 graphics card and present the approximate training time later in this section. The batch size is the largest

power of 2 that fits on the graphics card. We train the neural networks in PyTorch [Paszke et al., 2019] with the Adam optimization procedure from [Kingma and Ba, 2014]. We do not use weight decay (L2 regularization) since the model does not overfit. The initial learning rate for all models is 0.001 and decreases by a factor of 10 when losses stop decreasing for ten consecutive epochs. After five decreases, we stop the training procedure.

The most significant issue during training is the saturation of initial hidden values (see, e.g., [Glorot and Bengio, 2010] for a discussion of the effect of neuron saturation and weight initialization). The encoder and the decoder's output are respectively tanh and sigmoid activations, which have horizontal asymptotes and small derivatives for high magnitude inputs. All models use batch normalization, without which the embeddings saturate quickly. Initializing the network with large weights, using the techniques from [Glorot and Bengio, 2010], generated saturated embedding values of -1 or 1. To improve training, we initialize our models with very small weights, such that the average embedding value has a small variance and zero-centered. The neural network gradually increases the weights, so embeddings saturate less.

The activation functions for intermediate layers are hyperparameters; we compare tanh and rectified linear unit (ReLU). The ReLU activation function generated the best performances, but the models did not converge for every initial seed. Our selected models use ReLU, but sometimes required restarting the training process with a different initial seed if the embeddings saturate.

4.6   Training results

In this section, we provide results on the implementations of the four geographic embedding architectures, along with observations. Table 7 presents the training and validation reconstruction errors, along with the training time, the number of parameters and the mean embedding values.

	Training MSE	Validation MSE	Time	Parameters	Mean value
Small CRAE	0.21299473	0.21207126	5 hours	465 688	0.2051166
Large CRAE	0.21088413	0.20995240	3 days	55 622 416	0.6909323
Small CBOW-CRAE	0.21833613	0.21715157	2 hours	241 384	0.3463651
Large CBOW-CRAE	0.21731463	0.21609975	2 days	27 866 896	0.1174563

Table 7: Reconstruction errors from architectures

One cannot directly compare the reconstruction errors for the classic CRAE and CBOW-CRAE since classic CRAE reconstructs p^2 as many values as CBOW-CRAE. The average reconstruction error for CRAE is smaller than for CBOW-CRAE, which could be because the output of CBOW-CRAE does not have a determined equivalent vector in the input data. The CRAE model attempts to construct a one-to-one identity function for every neighbor because the input is identical to the output. On the other hand, CBOW-CRAE cannot exactly predict the values for a specific neighbor in the grid since there is no guarantee that the specific neighbor belongs to the same polygon as the central coordinate. One also notices that the validation data's reconstruction error is smaller than the training data, which is atypical in machine learning. However, changing the initial seed for training and validation data changes this relationship, so one attributes this effect to the specific data split. This also means that the model does not overfit on the training data: if it did, then the training error would be much smaller than the validation error. The lack of overfit is a result of the bottleneck dimension being small (8 or 16 dimensions) with respect to the dimension of the

input data (131 072).

For space and clarity reasons, we will not perform the explicit and implicit evaluations of embeddings. We do not find that one set of embeddings always performs better than the others, but find that the Large CBOW-CRAE behaves more appropriately, even if the reconstruction error is worse than for CRAE model. First, the average embeddings values for CBOW-CRAE models are closer to 0, which is desirable to increase the representation flexibility (especially within a GLM, because the range of embeddings is [-1, 1]). Attempts to manually correct these issues (normalization of embedding values after training) do not improve the quality of embeddings. In addition, the Large CBOW-CRAE had less saturated embedding dimensions, as we will discuss in the implicit evaluations. For these reasons, we continue our evaluation of embeddings with the Large CBOW-CRAE model, but we encourage researchers to experiment with other configurations.

4.7 Implicit evaluation of embeddings

We now implicitly evaluate if the 16 dimensions of the embeddings (generated by the Large CBOW-CRAE model) follows attribute 1 (TFL). Figure 10 presents an empty map for a location in Montréal (to identify points of interest), along with two embedding dimensions. The red star is the same coordinate as Figure 5. The map includes two rivers (in blue), an airport (bottom left), a mountain (bottom middle), and other parks. These points of interest typically have few surrounding postal codes, so the maps of embedding are less dense than heavily populated areas. The maps of embeddings include no legend because the magnitude of embeddings is irrelevant (regression weights will account for their scale). Not only are the embeddings smooth, but different dimensions

(a) Empty map   (b) Dimension 1   (c) Dimension 2
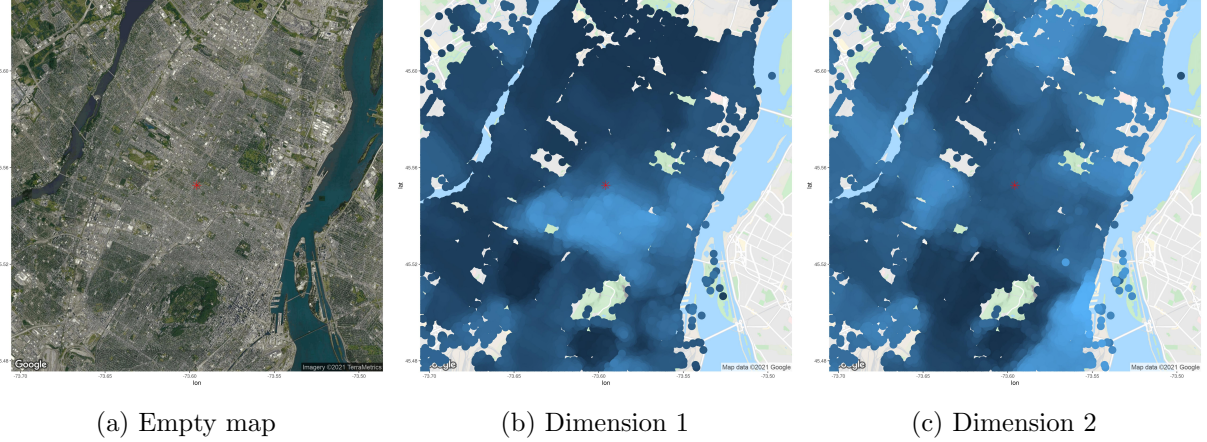
Figure 10: Visually inspecting embedding dimensions on a map for the Island of Montréal

learn different patterns. Recall that a polygon-based embedding model will learn the same shape (subject to the shape of polygons). Since models based on the geographic data cuboid depend on coordinates, the embeddings' shapes are more flexible. Inspecting Figures 10b and 10c around the red star, we observe that the embedding values form different shapes, and these shapes are different from the FSA polygons of Figure 6, validating attribute 2 (coordinate).

Visually inspecting the embeddings diagnosed an issue of embedding saturation, as discussed in Section 4.5. Saturated embeddings all equal the value -1 or 1, and because of the flat shape of the hyperbolic tangent activation function, the gradients of the model weights are too small for the

optimizer to correct the issue. In Figure 11, we present the histogram of the embedding values for dimensions 3, 4, 6, and the remaining dimensions combined. A good embedding will have values distributed along the entire support [-1, 1], as presented in Figure 11a. Dimensions 3 and 6 are heavily saturated, having most values equal exactly 1 or -1. If one includes embedding dimension 6 in a GLM, the feature will replicate the model intercept exactly (and cause collinearity issues if we include both). Embedding dimension 3 is less problematic since there is a small proportion of -1 values but still exhibits saturation. Most embedding values from dimension 4 are saturated at -1 but also have other values on the support of the activation function, which could provide useful information. We decide to discard embedding dimensions 3 and 6 for our applications.

(a) Other dimensions   (b) Dimension 3   (c) Dimension 4   (d) Dimension 6
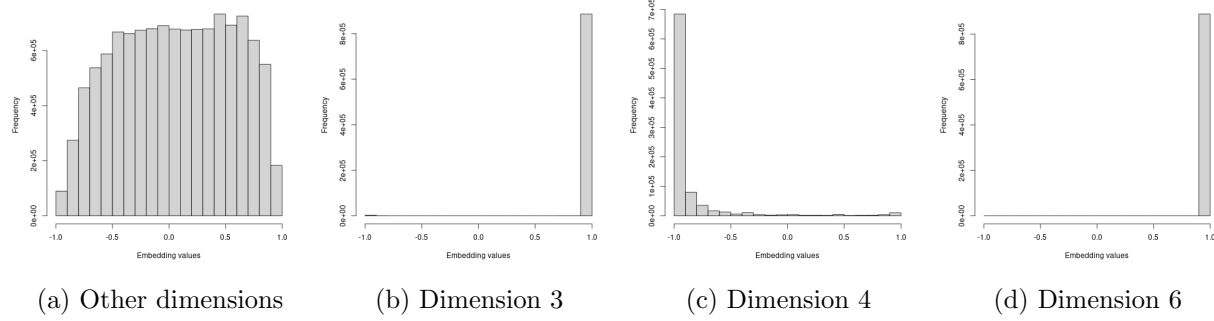
Figure 11: Histogram of embedding dimensions. Dimensions 3 and 6 are saturated

We visually conclude that the remaining embedding dimensions satisfy all desirable attributes 1 to 3 of geographic embeddings.

5 Applications

In this section, we present applications of predictive models for accident frequency. For all applications, we organize datasets as in Table 8. All applications are on Canadian data, so we project the coordinates to Atlas Lambert. Each observation also has geographic embeddings to describe the geography of the observation. The geographic embeddings remain the same, no matter the application: they correspond to the optimal Large CBOW-CRAE model trained in Section 4. Finally, we have typical non-geographic information like traditional actuarial features, the exposure and the response variable.

Index	Coordinates		Geographic embeddings			Other features			Exposure	Response
i	lon_i	lat_i	$\gamma^*_{i,1}$	$\ldots$	$\gamma^*_{i,\ell}$	x_{i1}	$\ldots$	x_{ip}	ω_i	y_i
1	lon_1	lat_1	$\gamma^*_{1,1}$	$\ldots$	$\gamma^*_{1,\ell}$	x_{11}	$\ldots$	x_{1p}	ω_1	y_1
2	lon_2	lat_2	$\gamma^*_{2,1}$	$\ldots$	$\gamma^*_{2,\ell}$	x_{21}	$\ldots$	x_{2p}	ω_2	y_2
$\vdots$	$\vdots$	$\vdots$	$\vdots$	$\ddots$	$\vdots$	$\vdots$	$\ddots$	$\vdots$	$\vdots$	$\vdots$
n	lon_n	lat_n	$\gamma^*_{n,1}$	$\ldots$	$\gamma^*_{n,\ell}$	x_{n1}	$\ldots$	x_{np}	ω_n	y_n

Table 8: Example of a geographic dataset with geographic embeddings

5.1 Dataset 1: Car accident counts

The first application is to predict car accident frequency in different postal codes on the island of Montréal between 2012 and 2017. The data comes from the *Société de l'assurance automobile du Québec* (SAAQ), the public insurance company for the province of Québec. The city of Montréal publishes a modified dataset including the coordinates of the closest intersection of the car accident (https://donnees.montreal.ca/ville-de-montreal/collisions-routieres). We then allocate the accidents to the nearest postal code. We organize data as in Table 8, with each observation representing one postal code. We use the years 2012 to 2016 for the training dataset, which contains 116 118 car accidents. We keep the year 2017 as an out-of-sample test dataset, containing 19 997 car accidents.

The model for the first application is a generalized additive model with a Poisson response to model the accident count. The relationship between the expected value of the response variable Y, the coordinates and the geographic embeddings is given by

$$\ln(E[Y_i]) = \beta_0 + \underbrace{f_k(lon_i,\ lat_i)}_{\text{spline component}} + \underbrace{\sum_{j=1}^{14} \gamma_{ij}^* \beta_j}_{\text{embedding component}}, \qquad i = 1, \ldots, n, \qquad (3)$$

where f_k is a bivariate spline function with $k \times k$ knots (in our application, a bivariate tensor product smooth, see [Wood, 2012] for details). The number of knots in the splines is a hyperparameter controlling flexibility. Model (3) contains a smooth geographic component from the bivariate spline, along with a linear geographic embedding component. One notices an advantage of geographic embeddings: instead of dealing with geographic coordinates directly, they capture geographic effects linearly with regression coefficients. Since geographic embeddings satisfy TFL, a linear combination of geographic embeddings also follows TFL. Geographic embeddings do not entirely replace geographic models: it is simple to combine traditional geographic models with the embeddings.

We compare the models with only the embedding component ($k = 0$ with embeddings), models with only spline components ($k > 0$ without embeddings), and combinations of embeddings and splines ($k > 0$ with embeddings). Table 9 presents the training deviance, test deviance, model degrees of freedom (DoF) and training time in seconds using the restricted maximum likelihood method using the mgcv R package. The DoF from the embedding component is constant at 14. For the spline component, we provide the effective DoF, which corresponds to the trace of the hat matrix of spline predictors; see [Wood, 2012] for details. The training times are based on a computer with Intel® Core™ i5-7600K CPU @ 3.80GHz.

One observes that for fixed k, including embeddings in the model decreases both train and test deviance. Increasing k, the number of knots in the spline component increases the effective DoF more than linearly. On the other hand, including the embedding component increases the effective DoF by 14 since embeddings' dimension remains the same. The number of knots needed in a spline model without embeddings to outperform the GLM without splines is $k = 7$, with 36.81 effective DoF. To improve model performance, it is generally more advantageous to add the embedding component than to increase the number of knots in the splines (based on the increase in effective DoF and the increase in training time).

To evaluate the embeddings extrinsically, one can study the statistical significance of the regression parameters. Table 10 presents the *p-values* for the regression parameters in the car accident

	Without embeddings				With embeddings γ^*			
k	Training	Test	DoF	Time (s)	Training	Test	DoF	Time (s)
0	–	–	–	–	153592	72419	15.00	0
3	156424	73247	8.98	2	153305	72349	20.53	5
5	156106	73237	18.39	3	152921	72205	32.58	5
8	153701	72353	45.25	10	151369	71550	59.19	11
10	152050	71822	78.03	74	150856	71374	80.13	13
15	149770	70859	155.39	66	149099	70612	166.49	71
20	147548	69818	263.76	341	146921	69589	275.58	148
25	144789	68602	410.49	328	144379	**68476**	420.32	607

Table 9: Performance comparison for car accident count models

count GLM model ($k = 0$ with embeddings). One notices that 13 embeddings have statistically significant regression at the 0.05 threshold, with 11 also statistically significant at the 10×10^{-5} level, which means that geographic embeddings capture useful features.

Parameter	*p-value*	Parameter	*p-value*	Parameter	*p-value*	Parameter	*p-value*
β_0	0.00000	β_4	0.00000	β_8	0.00355	β_{12}	0.00000
β_1	0.00000	β_5	0.00000	β_9	0.00000	β_{13}	0.00000
β_2	0.00000	β_6	0.00752	β_{10}	0.00000	β_{14}	0.00000
β_3	0.00000	β_7	0.00000	β_{11}	0.07549		

Table 10: *p*-values for car count GLM model

5.2 Dataset 2: Fire incident counts

The second application predicts fire incidents in different postal codes in Toronto between 2011 and July 2019. The data comes from City of Toronto Open Data (https://open.toronto.ca/dataset/fire-incidents/). The dataset contains the coordinates of the nearest major intersection of fire incidents, which we allocate to the nearest postal code. We organize data as in Table 8, with each observation representing one postal code. We use the years 2011 to 2017 for the training dataset, containing 12 540 incidents. We keep the year 2018 and the first half of 2019 as out-of-sample test dataset, containing 2 918 incidents.

The model for the second application is also a generalized additive model with a Poisson response. The relationship between the expected value of the response variable Y, the coordinate predictors and the geographic embeddings is still (3). Table 11 presents the training and test deviance, along with effective DoF and training time (still based on a computer with Intel® Core™ i5-7600K CPU @ 3.80GHz.). One draws similar conclusions to the first application: increasing k reduces the train and test deviance, and so does including geographic embeddings in the model. The number of knots needed in a spline model without embeddings to outperform the GLM without splines is $k = 8$, with 49.8 effective DoF.

In Table 12, we provide the *p-values* for the fire incident count GLM model ($k = 0$ with

	Without embeddings				With embeddings γ^*			
k	Training	Test	DoF	Time (s)	Training	Test	DoF	Time (s)
0	–	–	–	–	36323	13979	15	0
3	37622	14360	6.94	2	36161	13940	21.57	5
5	37084	14186	19.45	5	36019	13897	30.41	12
8	36480	13985	49.80	28	35840	13846	52.02	20
10	36371	13937	67.23	64	35628	13777	76.89	47
15	35414	13758	147.71	176	34814	13612	157.89	206
20	34461	13500	251.97	446	34046	13420	256.66	410
25	33713	13401	364.21	861	33312	**13319**	369.28	1413

Table 11: Performance comparison for fire incident models

embeddings). One notices that ten embeddings have statistically significant regression at the 0.05 threshold, with seven also statistically significant at the 10×10^{-5} level. In the car accident application, the only regression coefficient that was not significant at the 0.05 level was β_{11}, which is highly significant for the fire incidents frequency model.

Parameter	p-value	Parameter	p-value	Parameter	p-value	Parameter	p-value
β_0	0.00000	β_4	0.00000	β_8	0.13197	β_{12}	0.11907
β_1	0.00000	β_5	0.00000	β_9	0.00808	β_{13}	0.00000
β_2	0.05736	β_6	0.10260	β_{10}	0.01111	β_{14}	0.00000
β_3	0.00000	β_7	0.00000	β_{11}	0.00203		

Table 12: p-values for fire count model

The applications of datasets 1 and 2 compare the performance of geographic splines and geographic embeddings. One observes that GAMs without embeddings outperform GLMs with embeddings once the number of knots was sufficiently high. This finding is not surprising: the geographic embeddings in Section 4 depend on socio-demographic variables. Other geographic effects (meteorological, ecological, topological) could also affect the geographic risk. However, adding the embeddings to the model increased the performance, so that models should include embeddings for both datasets. One concludes that the geographic distribution of the population partially explains the geographic distribution of car accidents and fire incidents. Since residual effects (captured by the GAM splines) improve the model, socio-demographic information does not entirely explain the geographic distribution of risk. These conclusions hold for two highly populated cities (Montréal and Toronto) and for two predictive tasks that are not directly related to insurance, but which model P&C perils (car accident and fire incident counts).

5.3   Dataset 3: Home insurance

The third dataset contains historical losses of home insurance contracts for a portfolio in the province of Québec, Canada, between 2007 and 2011. The data comes from a large Canadian P&C insurance company and contains over 2 million observations. The home insurance contract covers six perils, including `fire`, `water` damage, sewer backup (`SBU`), wind & hail (`W&H`), `theft` and a final

category called `other`. The dataset provides the house's postal code for each observation, so we set the coordinates as the central point of the postal code and extract the embeddings from that same postal code. We also have traditional actuarial variables describing the house and the customer for each contract, along with the contract's length (exposure ω, treated as offsets in our models). We organize data as in Table 8, with each observation representing one insurance contract for one or fewer years. For illustration purposes, we select four traditional variables in the models, including x_1: age of the building, x_2: age of the client, x_3: age of the roof, and x_4: building amount.

The third application uses a GAM with a Poisson response to model the home claim frequency. The relationship between the response variable Y and the traditional variables, the geographic embeddings and the exposure is

$$\ln(E[Y_i]) = \beta_0 + \ln \omega + \underbrace{\sum_{j=1}^{4} x_{ij}\alpha_j}_{\text{traditional component}} + \underbrace{f_k(lon_i, \ lat_i)}_{\text{spline component}} + \underbrace{\sum_{j=1}^{14} \gamma_{ij}^*\beta_j}_{\text{embedding component}}, \qquad i = 1, \ldots, n. \quad (4)$$

The training times provided for all home insurance dataset comparisons are based on a computer with two Intel® Xeon® Processor E5-2683 v4 @2.10GHz (about 3.7 times faster than the i5 processor when running at full capacity).

5.3.1 Home accident frequency in Montréal

In the first comparison with the home insurance dataset, we attempt to predict the total claim frequency for an insurance contract on the island of Montréal. The training data are calendar year losses for 2007 to 2010, while the test data are the calendar year losses for 2011. Table 13 presents the training and test deviance, along with effective DoF and training time.

	Without embeddings				With embeddings γ^*			
k	Training	Test	DoF	Time (s)	Training	Test	DoF	Time (s)
0	–	–	–	–	66013	**14383**	19	58
3	66149	14390	6.69	242	65952	14399	23.70	483
5	65991	14400	16.49	108	65886	14402	33.61	1553
8	65838	14390	34.00	1306	65778	14388	48.65	1024
10	65766	14389	46.03	2201	65733	14388	58.21	1540
15	65691	14389	64.44	2533	65683	14391	73.42	3617
20	65652	14386	75.37	7733	65651	14387	82.29	12368
25	65644	14386	80.36	50902	65642	14387	86.39	50763

Table 13: Performance comparison for home total claim frequency models (Montréal)

The best model is the GLM with embeddings. Including splines with embeddings does not improve the model: although the training deviance decreases, the test deviance increases. One concludes that when smoothing the frequency of rare events with limited observations, splines learn patterns that overfit on observed loss experience and do not learn geographic effects that generalize to new observations. These conclusions are in contrast to the applications of Sections 5.1 and 5.2 (which had higher frequencies), where increasing the knots decreased the test deviance.

24

5.3.2 Home claim frequency in the entire portfolio

In the second comparison with the home insurance dataset, we train the ratemaking models on the entire province of Québec. This application is most representative of the ratemaking models in practice. We note that dataset 1 (Montréal) covered 365 km^2, dataset 2 (Toronto) covered 630 km^2, while this application covers almost 1 400 000 km^2, so the spline component will require a much larger number of knots to replicate the flexibility of the models in Sections 5.1, 5.2 and 5.3.1. Also, most of the area in Québec is uninhabited, so much of the flexibility is wasted on locations with no observations. The geographic embeddings in this application are the same as the previous applications, so the models with geographic embeddings have the same flexibility without significantly increasing the effective DoF. Table 14 presents the training and test deviance, along with effective DoF and training time for models. Note that we omit $k = 25$ since training the model would require too much RAM on the compute server.

k	Without embeddings				With embeddings $\boldsymbol{\gamma}^*$			
	Training	Test	DoF	Time (s)	Training	Test	DoF	Time (s)
0	–	–	–	–	332577	**80663**	19	312
3	333231	80766	7.18	4604	332422	80785	26.16	18158
5	332779	80767	18.63	5709	332251	80780	35.18	9809
8	332346	80837	43.97	17775	331948	80777	60.43	28823
10	331791	80771	64.89	41212	331550	80748	82.86	52041
15	331174	80853	126.60	37885	331025	80825	138.64	56316
20	330858	80852	181.65	59935	330763	80825	191.97	51102

Table 14: Performance comparison for home total claim frequency models (Province of Québec)

Once again, the best model is the GLM with embeddings. One observes a decreasing trend in the training deviance as k increases, but an increase in test deviance follows. One concludes that geographic embeddings capture all significant geographic risk, and splines overfit the training data without generalizing to new observations.

5.3.3 Extrinsic evaluation for home claim frequency

We now extrinsically evaluate geographic embeddings for predicting home insurance claim frequency. The home insurance contracts in our dataset cover six perils. We train seven GLM models with geographic embeddings and the four traditional variables: one for the total claims frequency and six for the claim frequency decomposed by individual peril. In Table 15, we present the *p-values* for the regression coefficients in the seven models, along with the number of times that the regression coefficients were significant at the 0.05 level (column #).

For clarity and simplicity, we use the abuse of terminology *significant embeddings* to mean that the regression coefficient associated with an embedding dimension is statistically significant, based on the *p-value*. One notices that the 12 embedding dimensions are significant for the majority of models, and that regression coefficients β_4 and β_5 are significant for all models. The signs of the regression coefficients (not shown for space) are not the same for every peril, meaning some embedding dimensions increase the expected claim frequency for certain perils but decrease it for

	Total	Fire	Theft	W&H	Water	SBU	Other	#
β_0	0.0000	0.1575	0.0009	0.0235	0.0000	0.0009	0.0000	6
β_1	0.0172	0.0204	0.0000	0.5152	0.0200	0.0001	0.0003	6
β_2	0.0000	0.8525	0.0198	0.0000	0.0000	0.0000	0.0000	6
β_3	0.0002	0.6756	0.0009	0.6661	0.3390	0.2551	0.0004	3
β_4	0.0169	0.0006	0.0000	0.0000	0.0000	0.0052	0.0027	7
β_5	0.0000	0.0050	0.0000	0.0000	0.0000	0.0000	0.0000	7
β_6	0.0033	0.0595	0.0018	0.0000	0.5091	0.0227	0.1292	4
β_7	0.0000	0.5498	0.0000	0.0000	0.3012	0.1538	0.0000	4
β_8	0.1695	0.0155	0.2429	0.0000	0.0007	0.4392	0.0040	4
β_9	0.0063	0.7287	0.6080	0.0033	0.0662	0.1104	0.8288	2
β_{10}	0.0000	0.3631	0.0001	0.2265	0.0000	0.5243	0.0009	4
β_{11}	0.0690	0.0032	0.0000	0.7296	0.0000	0.0051	0.9000	4
β_{12}	0.0000	0.0038	0.2538	0.2029	0.0000	0.0002	0.0000	5
β_{13}	0.0000	0.0000	0.0000	0.8895	0.0000	0.0012	0.0000	6
β_{14}	0.5908	0.0172	0.0000	0.0000	0.7580	0.0000	0.0318	5
α_1	0.0028	0.0001	0.0514	0.0000	0.2503	0.0000	0.0000	5
α_2	0.0000	0.0000	0.0000	0.5023	0.0000	0.0000	0.0000	6
α_3	0.0000	0.2040	0.2510	0.0000	0.0005	0.0000	0.0004	5
α_4	0.0000	0.1022	0.0000	0.5681	0.0000	0.0000	0.0000	5

Table 15: *p-values* for the GLMs by peril

other perils.

The peril GLMs with the most significant geographic embeddings are `theft` and `other`. Since the embeddings capture socio-demographic effects, it makes sense that the `theft` peril, which one mostly associates with socio-demographic actions, has the highest number of significant embeddings. The authors have no knowledge of the contents of the `other` peril so we avoid interpreting this result. The perils with the least number of significant embeddings are `fire` and `W&H`. One notices that wind and hail are a meteorological phenomena, making sense that geographic embeddings, build on socio-demographic variables, are not all significant. One concludes that geographic embeddings generate statistically significant regression coefficients, so they are useful for ratemaking models. This conclusion holds when deconstructing the claim frequency into individual perils.

5.3.4 Predicting in a new territory

In the third comparison with the home insurance dataset, we determine if embeddings can predict geographic risk in a territory with no historical losses. On the one hand, we train a GLM with embeddings on a dataset with no historical losses from a sub-territory. On the other hand, we train a GLM with embeddings or a GAM with bivariate splines on a dataset with observations exclusively from that sub-territory. Then, we compare the performance of both approaches. To study this question, we split the dataset into two territories; Figure 12 illustrates an example for the island of Montréal. The polygon in blue represents the island of Montreal (see Figure 12a for a focused look on the island), and in red is the remainder of the province (see Figure 12b for the entire province, with Montréal in blue at the bottom left). We train a Poisson GLM with embeddings for the two datasets: model OOT (out of territory) trains on all observations in the province except

(a) Zoomed in   (b) Zoomed out
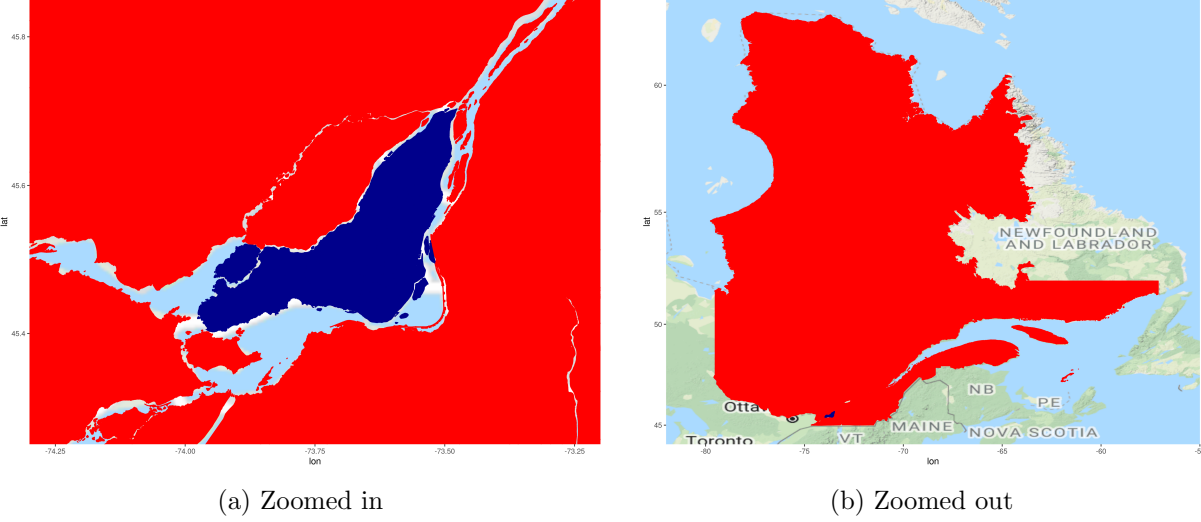
Figure 12: Blue (darkest): Island of Montréal, red (lightest): Rest of Québec.

Montréal (red area), while model WT (within the territory) trains on observations in Montréal (blue area). Therefore, model OOT never saw any observations from Montréal. We also train a Poisson GAM with $k = 10$ as a baseline. All models use 2007 to 2010 calendar years for training data. Then, we compare the performance of the models on Montréal in 2011 (blue territory). The test deviance for model OOT is 14364, while the test deviance for model WT is 14383. In Table 16, we reproduce the results for the population centers in Québec with a population of over 100 000 and present the deviance computed on 2011 data.

Population center	WT	OOT	GAM	Population center	WT	OOT	GAM
Montréal	14383	**14364**	14400	Sherbrooke	2783	**2754**	2782
Québec	3803	**3787**	3801	Saguenay	961	**958**	963
Laval	**4043**	4046	4043	Levis	2505	**2500**	2500
Gatineau	6495	**6406**	6495	Trois Rivières	2961	**2952**	2961
Longueuil	**3184**	3203	3185	Terrebonne	2674	**2656**	2677

Table 16: Test deviance with different training datasets by population centers

The models trained with OOT typically have smaller test deviance, so generalize better. For a few population centers, it is more beneficial to use data from the actual territory, but GLMs with geographic embeddings still outperform GAMs. These results lead to an important conclusion: to predict geographic risk in a sub-territory of a dataset, it is more advantageous to use geographic embeddings on a model trained with a larger quantity of losses, no matter where these losses occur, than to train a model using data from the sub-territory exclusively. When performing territorial ratemaking with traditional methods like GAMs, one typically focuses on one sub-territory at a time, thus ignores the remainder of the training data. On the other hand, OOT models use much larger datasets than the WT or GAM models, and this increased volume is more beneficial to improve the predictive performance than only studying the information from the territory of interest. This means that a model using geographic embeddings on a large quantity of information can improve geographic prediction in a territory with no historical losses better than if one had historical losses. In practice, one would not intentionally omit the observations in a sub-territory

27

to predict the geographic risk: we construct this comparison to show that GLMs with embeddings can predict the geographic risk in territories with no historical losses.

6   Conclusion and Discussion

This paper shows that geographic models (bivariate splines) are unnecessary to capture the geographic distribution of risk. Instead, we can first capture the population's geographic distribution within a geographic representation learning model that outputs a vector of values. Using this vector in a simpler model such as a GLM predicts the geographic risk of home insurance losses more accurately than explicit geographic GAMs and enables predicting losses in territories with no historical losses.

The ideas of Sections 3 and 4 require much technical knowledge on neural networks and geographic models. These skills are outside of the typical actuary's knowledge, although this is rapidly changing. One main advantage of the geographic embedding approach is that another can use them within any predictive model after constructing the geographic embeddings. In both applications of Section 5, we use the same set of embeddings for postal codes; we did not need to create specific representations for specific applications since we keep the geographic embeddings general. This could lead to a new relationship between actuaries, other domain experts and data scientists: one of a streamlined process of creating representations of novel sources of data, followed by actuarial modeling within existing models, akin to an assembly line.

Training the embeddings in Section 4 required no knowledge of the insurance industry nor insurance data. The resulting embeddings are a geographic compression of socio-demographic information from census data. For this reason, the same set of embeddings could also be used for other tasks in domains where socio-demographic information could be useful, including life insurance, urban planning, election forecasting and crime rate prediction.

Note that embeddings do not entirely replace geographic models: they provide a simple way of compressing socio-demographic data into a vector. In some cases, GLMs using geographic embeddings are useful enough to avoid complex geographic models. In others, they provide a simple vector of features such that ratemaking models perform well.

We offer two justifications of why we believe geographic embeddings work so well. First, the embeddings geographically capture geographic patterns that represent census information on a location and its neighbors. Since human-generated risks are closely related to human information, the geographic distribution of census embeddings will likely be related to the geographic distribution of risks. Therefore, a model using the census embeddings, even one as simple as a GLM, will be capable of modeling geographic risk. Second, insurance data is inherently noisy, so a model requires a high volume of historical losses to generate credible predictions. To build a geographic model, one can only use a subset of data to learn the geographic effect: the size of territories must be large enough to achieve credibility. When using geographic embeddings, the same features are used for the entire model, so the regression parameters associated with the geographic embeddings achieve credibility faster by using fewer parameters. One can interpret these two claims as follows: observations from Montréal can help predict the geographic risk in Québec since they both use the same geographic features. If an embedding dimension in Montréal generates higher risk, a GLM will capture this effect. An observation in Québec with a similar embedding dimension will predict a similarly higher risk, making sense because similar embedding dimensions imply similar census

data, meaning the same type of individuals inhabits both places so that the socio-demographic risks will be similar.

We proposed one intrinsic evaluation for geographic embeddings. For more, we could look at the field of natural language processing (NLP), where embeddings are used for many applications [Mikolov et al., 2017]. Researchers in this field have developed a set of tasks to evaluate the quality of embeddings. A common intrinsic evaluation task for natural language processing is computing a similarity distance between different two word embeddings and comparing the results with human similarity ratings from datasets like wordsim353 [Finkelstein et al., 2002]. One can also compare the similarity between different locations. For example, select three coordinates: two from similar territories and one from a dissimilar one. Embeddings intrinsically make sense if the similar territories have a smaller cosine distance than with the dissimilar embedding. This task depends on human interpretation, so without a survey asking many participants to rate the similarity of various territories, this intrinsic evaluation is not reliable for geographic embeddings. Future work on geographic embeddings could perform such a survey for an additional intrinsic evaluation.

7 Acknowledgments

References

[Anselin et al., 2010] Anselin, L., Syabri, I., and Kho, Y. (2010). Geoda: an introduction to spatial data analysis. In *Handbook of Applied Spatial Analysis*, pages 73–89. Springer.

[Bengio et al., 2013] Bengio, Y., Courville, A., and Vincent, P. (2013). Representation learning: A review and new perspectives. *IEEE Transactions on Pattern Analysis and Machine Intelligence*, 35(8):1798–1828.

[Blier-Wong et al., 2020] Blier-Wong, C., Baillargeon, J.-T., Cossette, H., Lamontagne, L., and Marceau, E. (2020). Encoding neighbor information into geographical embeddings using convolutional neural networks. In *The Thirty-Third International Flairs Conference*.

[Blier-Wong et al., 2021a] Blier-Wong, C., Baillargeon, J.-T., Cossette, H., Lamontagne, L., and Marceau, E. (2021a). Rethinking representations in P&C actuarial science with deep neural networks. *arXiv preprint arXiv:2102.05784*.

[Blier-Wong et al., 2021b] Blier-Wong, C., Cossette, H., Lamontagne, L., and Marceau, E. (2021b). Machine learning in P&C insurance: A review for pricing and reserving. *Risks*, 9(1):4.

[Boskov and Verrall, 1994] Boskov, M. and Verrall, R. (1994). Premium rating by geographic area using spatial models. *ASTIN Bulletin: The Journal of the IAA*, 24(1):131–143.

[Cocos and Callison-Burch, 2017] Cocos, A. and Callison-Burch, C. (2017). The language of place: Semantic value from geospatial context. In *Proceedings of the 15th Conference of the European Chapter of the Association for Computational Linguistics: Volume 2, Short Papers*, pages 99–104.

[Collobert and Weston, 2008] Collobert, R. and Weston, J. (2008). A unified architecture for natural language processing: Deep neural networks with multitask learning. In *Proceedings of the 25th International Conference on Machine Learning*, pages 160–167.

[Corbett-Davies and Goel, 2018] Corbett-Davies, S. and Goel, S. (2018). The Measure and Mismeasure of Fairness: A Critical Review of Fair Machine Learning. *arXiv:1808.00023 [cs]*.

[Cressie, 1990] Cressie, N. (1990). The origins of kriging. *Mathematical Geology*, 22(3):239–252.

[Cressie, 2015] Cressie, N. (2015). *Statistics for Spatial Data*. John Wiley & Sons.

[Denuit and Lang, 2004] Denuit, M. and Lang, S. (2004). Non-life rate-making with bayesian gams. *Insurance: Mathematics and Economics*, 35(3):627–647.

[Devlin et al., 2019] Devlin, J., Chang, M.-W., Lee, K., and Toutanova, K. (2019). BERT: Pre-training of Deep Bidirectional Transformers for Language Understanding. *arXiv:1810.04805 [cs]*.

[Diggle and Ribeiro, 2007] Diggle, P. and Ribeiro, P. J. (2007). *Model-Based Geostatistics*. Springer series in statistics. Springer.

[Diggle, 2013] Diggle, P. J. (2013). *Statistical Analysis of Spatial and Spatio-temporal Point Patterns*. CRC Press.

[Dimakos and Di Rattalma, 2002] Dimakos, X. K. and Di Rattalma, A. F. (2002). Bayesian premium rating with latent structure. *Scandinavian Actuarial Journal*, 2002(3):162–184.

[Du et al., 2019] Du, J., Zhang, Y., Wang, P., Leopold, J., and Fu, Y. (2019). Beyond geo-first law: Learning spatial representations via integrated autocorrelations and complementarity. In *2019 IEEE International Conference on Data Mining (ICDM)*, pages 160–169. IEEE.

[Eisenstein et al., 2010] Eisenstein, J., O'Connor, B., Smith, N. A., and Xing, E. P. (2010). A latent variable model for geographic lexical variation. In *Proceedings of the 2010 Conference on Empirical Methods in Natural Language Processing*, pages 1277–1287. Association for Computational Linguistics.

[Fahrmeir et al., 2003] Fahrmeir, L., Lang, S., and Spies, F. (2003). Generalized geoadditive models for insurance claims data. *Blätter der DGVFM*, 26(1):7–23.

[Finkelstein et al., 2002] Finkelstein, L., Gabrilovich, E., Matias, Y., Rivlin, E., Solan, Z., Wolfman, G., and Ruppin, E. (2002). Placing Search in Context: The Concept Revisited. *ACM Transactions on Information Systems*, 20(1):16.

[Firth, 1957] Firth, J. R. (1957). A synopsis of linguistic theory, 1930-1955. *Studies in linguistic analysis*.

[Frees, 2015] Frees, E. W. (2015). Analytics of insurance markets. *Annual Review of Financial Economics*, 7:253–277.

[Fu et al., 2019] Fu, Y., Wang, P., Du, J., Wu, L., and Li, X. (2019). Efficient Region Embedding with Multi-View Spatial Networks: A Perspective of Locality-Constrained Spatial Autocorrelations. *Proceedings of the AAAI Conference on Artificial Intelligence*, 33:906–913.

[Getis, 2010] Getis, A. (2010). Spatial autocorrelation. In *Handbook of Applied Spatial Analysis*, pages 255–278. Springer.

[Glorot and Bengio, 2010] Glorot, X. and Bengio, Y. (2010). Understanding the difficulty of training deep feedforward neural networks. In *Proceedings of the 13th International Conference on Artificial Intelligence and Statistics (AISTATS) 2010*, page 8, Sardinia, Italy.

[Goodfellow et al., 2016] Goodfellow, I., Bengio, Y., and Courville, A. (2016). *Deep Learning*. MIT press.

[Gschlößl and Czado, 2007] Gschlößl, S. and Czado, C. (2007). Spatial modelling of claim frequency and claim size in non-life insurance. *Scandinavian Actuarial Journal*, 2007(3):202–225.

[Han et al., 2011] Han, J., Pei, J., and Kamber, M. (2011). *Data Mining: Concepts and Techniques*. Elsevier.

[Harris, 1954] Harris, Z. S. (1954). Distributional structure. *Word*, 10(2-3):146–162.

[He et al., 2016] He, K., Zhang, X., Ren, S., and Sun, J. (2016). Deep residual learning for image recognition. In *Proceedings of the IEEE Conference on Computer Vision and Pattern Recognition*, pages 770–778.

[Henckaerts et al., 2018] Henckaerts, R., Antonio, K., Clijsters, M., and Verbelen, R. (2018). A data driven binning strategy for the construction of insurance tariff classes. *Scandinavian Actuarial Journal*, 2018(8):681–705.

[Hengl et al., 2007] Hengl, T., Heuvelink, G. B., and Rossiter, D. G. (2007). About regression-kriging: From equations to case studies. *Computers & Geosciences*, 33(10):1301–1315.

[Hui et al., 2020] Hui, B., Yan, D., Ku, W.-S., and Wang, W. (2020). Predicting economic growth by region embedding: A multigraph convolutional network approach. In *Proceedings of the 29th ACM International Conference on Information & Knowledge Management*, pages 555–564.

[Ioffe and Szegedy, 2015] Ioffe, S. and Szegedy, C. (2015). Batch normalization: Accelerating deep network training by reducing internal covariate shift. In *International Conference on Machine Learning*, pages 448–456. PMLR.

[ISO 19109, 2015] ISO 19109 (2015). Geographic information — rules for application schema. Standard, International Organization for Standardization, Geneva. Technical Committee ISO/TC 211, Geographic Information/Geomatics.

[Jeawak et al., 2019] Jeawak, S. S., Jones, C. B., and Schockaert, S. (2019). Embedding geographic locations for modelling the natural environment using Flickr tags and structured data. In *European Conference on Information Retrieval*, pages 51–66. Springer.

[Jenkins et al., 2019] Jenkins, P., Farag, A., Wang, S., and Li, Z. (2019). Unsupervised Representation Learning of Spatial Data via Multimodal Embedding. In *Proceedings of the 28th ACM International Conference on Information and Knowledge Management*, pages 1993–2002, Beijing China. ACM.

[Jurafsky and Martin, 2009] Jurafsky, D. and Martin, J. H. (2009). *Speech & Language Processing*. Pearson Education, second edition.

[Kingma and Ba, 2014] Kingma, D. P. and Ba, J. (2014). Adam: A method for stochastic optimization. *arXiv preprint arXiv:1412.6980*.

[Kusner et al., 2018] Kusner, M. J., Loftus, J. R., Russell, C., and Silva, R. (2018). Counterfactual Fairness. *arXiv:1703.06856 [cs, stat]*.

[Lambert, 1772] Lambert, J. H. (1772). Beiträge zum gebrauche der mathematik und deren anwendung: Part iii, section 6: Anmerkungen und zusätze zur entwerfung der land-und himmelscharten: Berlin, translated and introduced by wr tobler, univ. *Translated and introduced by WR Tobler, Univ. Michigan in 1972*.

[Lindholm et al., 2020] Lindholm, M., Richman, R., Tsanakas, A., and Wuthrich, M. V. (2020). Discrimination-free insurance pricing. *Available at SSRN : 3520676*.

[Matheron, 1965] Matheron, G. (1965). *Les Variables Régionalisées et leur Estimation: une Application de la Théorie de Fonctions Aléatoires aux Sciences de la Nature*, volume 4597. Masson et CIE.

[Mikolov et al., 2013] Mikolov, T., Chen, K., Corrado, G., and Dean, J. (2013). Efficient estimation of word representations in vector space. *arXiv preprint arXiv:1301.3781*.

[Mikolov et al., 2017] Mikolov, T., Grave, E., Bojanowski, P., Puhrsch, C., and Joulin, A. (2017). Advances in pre-training distributed word representations.

[Miller, 2004] Miller, H. J. (2004). Tobler's first law and spatial analysis. *Annals of the Association of American Geographers*, 94(2):284–289.

[Paszke et al., 2017] Paszke, A., Gross, S., Chintala, S., Chanan, G., Yang, E., DeVito, Z., Lin, Z., Desmaison, A., Antiga, L., and Lerer, A. (2017). Automatic differentiation in pytorch. In *31st Conference on Neural Information Processing Systems*.

[Paszke et al., 2019] Paszke, A., Gross, S., Massa, F., Lerer, A., Bradbury, J., Chanan, G., Killeen, T., Lin, Z., Gimelshein, N., Antiga, L., et al. (2019). Pytorch: An imperative style, high-performance deep learning library. *arXiv preprint arXiv:1912.01703*.

[R Core Team, 2020] R Core Team (2020). *R: A Language and Environment for Statistical Computing*. R Foundation for Statistical Computing, Vienna, Austria.

[Richman, 2020] Richman, R. (2020). AI in actuarial science – a review of recent advances – part 2. *Annals of Actuarial Science*, pages 1–29.

[Saeidi et al., 2015] Saeidi, M., Riedel, S., and Capra, L. (2015). Lower dimensional representations of city neighbourhoods. In *Workshops at the Twenty-Ninth AAAI Conference on Artificial Intelligence*.

[Shalev-Shwartz and Ben-David, 2014] Shalev-Shwartz, S. and Ben-David, S. (2014). *Understanding Machine Learning: From Theory to Algorithms*. Cambridge University Press.

[Shi and Shi, 2017] Shi, P. and Shi, K. (2017). Territorial risk classification using spatially dependent frequency-severity models. *ASTIN Bulletin: The Journal of the IAA*, 47(2):437–465.

[Simonyan and Zisserman, 2014] Simonyan, K. and Zisserman, A. (2014). Very deep convolutional networks for large-scale image recognition. *arXiv preprint arXiv:1409.1556*.

[Snyder, 1987] Snyder, J. P. (1987). *Map projections–A working manual*, volume 1395. US Government Printing Office.

[Taylor, 2001] Taylor, G. (2001). Geographic premium rating by Whittaker spatial smoothing. *ASTIN Bulletin: The Journal of the IAA*, 31(1):147–160.

[Taylor, 1989] Taylor, G. C. (1989). Use of spline functions for premium rating by geographic area. *ASTIN Bulletin: The Journal of the IAA*, 19(1):91–122.

[Tobler, 1970] Tobler, W. R. (1970). A computer movie simulating urban growth in the Detroit region. *Economic Geography*, 46(sup1):234–240.

[Torge and Müller, 2012] Torge, W. and Müller, J. (2012). *Geodesy*. Walter de Gruyter.

[Wackernagel, 2013] Wackernagel, H. (2013). *Multivariate geostatistics: An introduction with applications*. Springer Science & Business Media.

[Wang et al., 2017] Wang, C., Schifano, E. D., and Yan, J. (2017). Geographical Ratings with Spatial Random Effects in a Two-Part Model. *Variance*, 13(1):20.

[Wang et al., 2020] Wang, Z., Li, H., and Rajagopal, R. (2020). Urban2Vec: Incorporating Street View Imagery and POIs for Multi-Modal Urban Neighborhood Embedding. *Proceedings of the AAAI Conference on Artificial Intelligence*, 34(01):1013–1020.

[Wood, 2012] Wood, S. (2012). mgcv: Mixed GAM computation vehicle with GCV/AIC/REML smoothness estimation.

[Xu et al., 2020] Xu, S., Cao, J., Legg, P., Liu, B., and Li, S. (2020). Venue2Vec: An Efficient Embedding Model for Fine-Grained User Location Prediction in Geo-Social Networks. *IEEE Systems Journal*, 14(2):1740–1751.

[Yao et al., 2017] Yao, Y., Li, X., Liu, X., Liu, P., Liang, Z., Zhang, J., and Mai, K. (2017). Sensing spatial distribution of urban land use by integrating points-of-interest and Google Word2Vec model. *International Journal of Geographical Information Science*, 31(4):825–848.

[Yin et al., 2019] Yin, Y., Liu, Z., Zhang, Y., Wang, S., Shah, R. R., and Zimmermann, R. (2019). GPS2Vec: Towards Generating Worldwide GPS Embeddings. In *Proceedings of the 27th ACM SIGSPATIAL International Conference on Advances in Geographic Information Systems*, pages 416–419, Chicago IL USA. ACM.

[Zhang et al., 2019] Zhang, Y., Fu, Y., Wang, P., Li, X., and Zheng, Y. (2019). Unifying inter-region autocorrelation and intra-region structures for spatial embedding via collective adversarial learning. In *Proceedings of the 25th ACM SIGKDD International Conference on Knowledge Discovery & Data Mining*, pages 1700–1708.

A Canadian census details

In this section, we present the categories of variables that are available for every FSA in the Canadian census data. We exclude the variables from the categories denoted with an asterisk (*).

1. Population and dwellings
2. Age characteristics
3. Household and dwelling characteristics
4. Marital status
5. Family characteristics
6. Household type
7. Knowledge of official languages*
8. First official language spoken*
9. Mother tongue*
10. Language spoken most often at home*
11. Other language spoken regularly at home*
12. Income of individuals in 2015
13. Income of households in 2015
14. Income of economic families in 2015
15. Low income in 2015
16. Knowledge of languages*
17. Citizenship*
18. Immigrant status and period of immigration*
19. Age at immigration*
20. Immigrants by selected place of birth*
21. Recent immigrants by selected places of birth*
22. Generation status*
23. Admission category and applicant type*
24. Aboriginal population*
25. Visible minority population*
26. Ethnic origin population*
27. Household characteristics
28. Highest certificate, diploma or degree
29. Major field of study - Classification of Instructional Programs (CIP) 2016
30. Location of study compared with province or territory of residence with countries outside Canada*
31. Labour force status
32. Work activity during the reference year
33. Class of worker
34. Occupation - National Occupational Classification (NOC) 2016
35. Industry - North American Industry Classification System (NAICS) 2012
36. Place of work status
37. Commuting destination
38. Main mode of commuting
39. Commuting duration
40. Time leaving for work
41. Language used most often at work
42. Other language used regularly at work
43. Mobility status - Place of residence 1 year ago
44. Mobility status - Place of residence 5 years ago